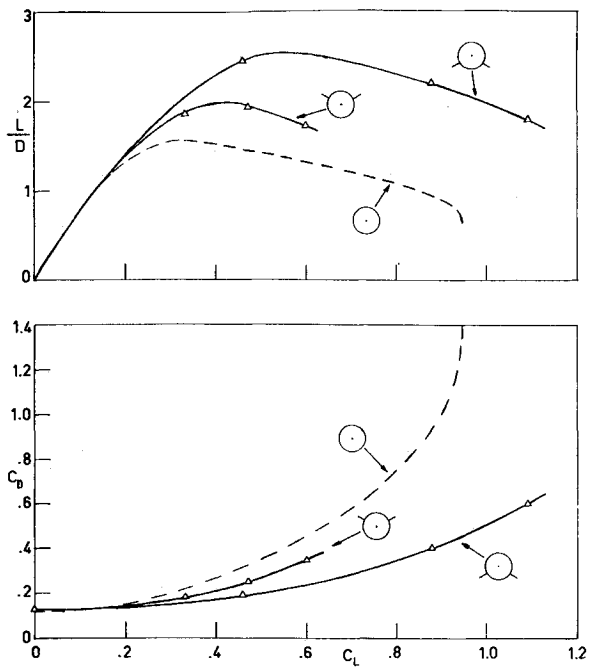

Fig. 4 Drag coefficient and life-drag ratio vs lift coefficient.

tive angle of attack (negative dihedral); the cross flow component on the windward side remains very small and the pressure results nearly constant in this region. On the leeward side the expansion on the back of the wing produces a region of low pressure on the cone; far from the wing (about 20° in this case) the interference practically disappears and the pressure distribution becomes similar to that obtained for an isolated cone. As a comparison, the pressure distribution computed with the Newtonian approximation for a 20° cone is also plotted. The larger pressure on the windward side acts to increase both the lift and the drag of the cone, whereas the expansion induced near the back of the wing acts practically only to reduce the drag (because in the region near $\theta = 90°$ the contribution of the pressure to the lift is very small). At negative angles of attack (positive dihedral) the interference effect of the wing appears to be less pronounced; this is explained by the fact that the wing is partially shaded by the cone surface. There is still a reduction in the cross flow and an increase of pressure on the windward side, especially near the wing, but this actually gives a negative contribution to the lift while the drag is increased.

The pressure on the wing was also measured; at angles of attack larger than 5° the pressure results practically constant on the whole wing surface. Due to the interference with the cone, the load on the wing results larger than the load on an isolated wing at the same angle of attack.

Direct measurements of the lift and the drag were performed with a three-component sting balance at several angles of attack from −16° to 20°; the results are shown in Figs. 3 and 4. In order to compare the present results with the simple cone configuration, the experimental lift and drag coefficients for a 20° cone[1] are also plotted. In Fig. 3 the lift coefficient and the drag coefficient are plotted against the angle of attack. The values of the lift coefficient computed from the pressure distribution are in good agreement with the balance measurements, so that it appears that the effect of the skin friction and the base drag on the lift is very small compared to the pressure force. Comparing with the isolated cone, it can be seen that a large increase in lift is obtained with the negative dihedral configuration, whereas the positive dihedral gives only a rather small increase. The positive dihedral configuration has a drag coefficient practically equivalent to that of the isolated cone, whereas the negative dihedral has a rather larger drag, especially at large angle of attack. The drag coefficient measured with the balance is larger than that computed from the pressure distribution; the difference (sum of the viscous drag and the base drag) decreases as the angle of attack increases. The viscous drag coefficient has been computed at zero angle of attack, assuming a completely turbulent boundary layer and using the reference enthalpy method; the result is equal to about 0.018; the base pressure coefficient results equal to about 0.04[2]; the sum is equal to 0.058, and it is in good agreement with the experimental results.

A more indicative idea of the difference between the characteristics of the wing-cone configuration and the isolated cone is obtained considering the polar diagram. Figure 4 shows that the polar of the negative dihedral configuration is much flatter than those of the cone and the positive dihedral, especially for large values of C_L. The lift-drag ratio is also plotted in Fig. 4; it appears that the negative dihedral configuration gives a much larger lift-drag ratio than the simple cone and the difference increases with C_L; the positive dihedral configuration gives only a moderate gain with a maximum at about $C_L = 0.5$, whereas for increasing C_L it tends to behave like the cone.

References

[1] Wells, W. R. and Armstrong, W. O., "Tables of Aerodynamic Coefficients obtained from Developed Newtonian Expressions for Complete and Partial Conic and Spheric Bodies at Combined Angles of Attack and Sideslip with some Comparisons with Hypersonic Experimental Data," TR R-127, 1962, NASA.

[2] Zarin, N. A., "Base Pressure Measurements on Sharp and Blunt 9° Cones at Mach Numbers from 3.50 to 9.20," *AIAA Journal*, Vol. 4, No. 4, April 1966, pp. 743–745.

Preionization and Velocity Effects in MHD Channels with Nonequilibrium Plasmas

Lajos L. Lengyel*
Institut für Plasmaphysik, Garching bei München, Germany

RESULTS of numerical computations pertaining to current and potential distributions in MHD channels are reported herein. Unlike in previous studies (see, for example, Refs. 1 and 2) no periodic field distributions have been assumed here. The computations were performed for a Faraday-type channel with a given finite number of electrode pairs. A two-dimensional approximation is used: $\partial/\partial z \equiv 0$, $v \parallel \hat{x}$, and $\mathbf{B} = \text{const} \parallel \hat{z}$. The axial current component was assumed to vanish at upstseam and downstream "infinities." In the mathematical model previously developed for a potassium seeded argon plasma[1,3] allowance is made for nonequilibrium ionization, finite rate recombination,[4] thermal conductivity of the electron gas, and the effect of inelastic collisions on the energy balance of the electrons. A value of 10 was assigned to the inelastic collision loss factor[5] (the magnitude of this coefficient affects primarily the ideal conductivity value and not the relative magnitudes of the preionization and velocity effects). The constant and uniform magnetic field was intentionally kept low enough to avoid nonconvergent (fluctuating) solutions and results whose interpretation may involve speculation. A uniform electron density is prescribed at a certain distance upstream of the first elec-

Received September 9, 1970; revision received November 10, 1970.

* Staff Scientist.

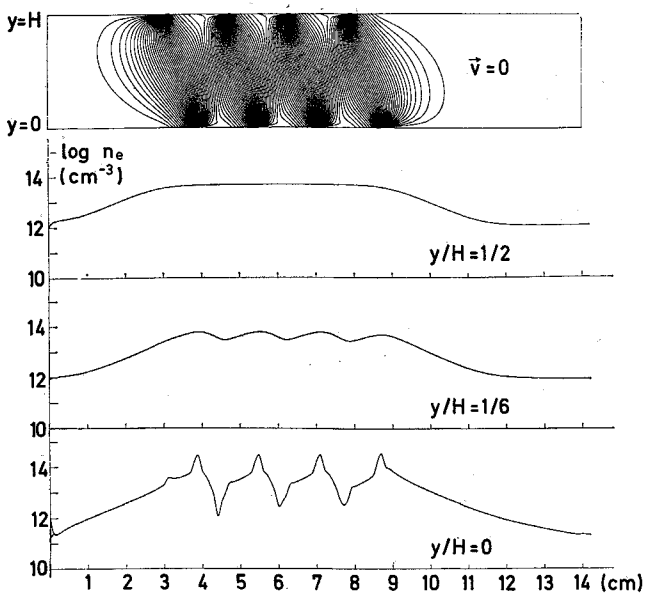

Fig. 1 Current pattern and electron density distributions at negligible gas velocity.

trode pair; it may be equal to or higher than the equilibrium value corresponding to the given (average) gas temperature. Electrode losses (sheaths, emission phenomena, etc.) are not taken into account. The gas velocity and temperature profiles are given by $v/v_0 = (T_g - T_w)/T_0 - T_w) = [4y(1 - y/H)/H]^{0.2}$ where v_0 and T_0 are the gas velocity and temperature at the channel axis, and T_w represents the wall temperature.

The two-dimensional boundary-value problem formulated for the current distribution[1,3] is supplemented by the boundary conditions $J_{\text{norm}} = 0$ at insulator surfaces, $E_{\tan} = 0$ at electrode surfaces, and $n_e \approx n_{e0}$ at $x = 0$ (a prescribed uniform electron density at the inlet section). Furthermore, the insulator sections upstream of the first and downstream of the last electrode pairs are chosen long enough to satisfy the conditions $J_x \approx 0$, $T_e \approx T_g$ and $\partial T_e/\partial x \approx 0$ at $x = 0$, and $x = x_{\text{exit}}$ (conditions at upstream and downstream "infinities").

In the process of solution, which is an iterative solution of

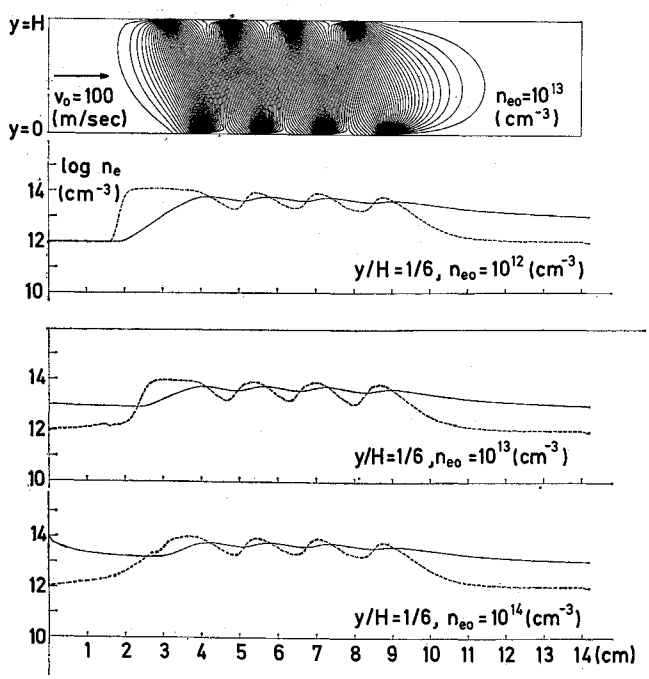

Fig. 2 A typical current distribution and three electron density distributions corresponding to three different inlet electron densities at $v_0 = 100$ m/sec.

the linearized second-order partial differential equation written for the current stream function,[1,3] the effect of the boundaries on the electron gas has been neglected. Such an approximation appeared to be necessary in order to avoid solving a set of coupled two-dimensional boundary-value problems, which, because of the lack of mathematically simple and physically plausible boundary conditions on n_e and T_e, exceeds the aim of the present study.

Results of Computations

Computations were performed for a potassium seeded argon plasma (0.2% seed concentration) at atmospheric pressure with $T_0 = 1800°$K, $T_w = 1600°$K, $B = 0.16$ tesla, $H = 3$ cm, $S = 1.6$ cm, and $C = 0.8$ cm, where H is the channel height, S is the distance from the midpoint of an insulator segment to the midpoint of the next one measured in the axial (x) direction, and C is the width of an electrode. Four pairs of electrodes were considered, and a total current of 1.6 amp was sent through each electrode pair. A series of numerical tests have shown that on the upstream side of the electrodes the conditions characterizing "infinity" are reached, with a satisfactory degree of accuracy, at a distance of ~ 3 cm in front of the first electrode pair. Because of the velocity effects, a somewhat larger distance is required for reaching "infinity" on the downstream side. A mesh size of 0.1 cm has been used in all calculations.

Machine plots representing the current streamlines and the distribution of the electron density at three y = const lines are shown in Fig. 1 for negligible gas velocity ($v \approx 0$). The inlet electron density n_{e0} corresponds to Saha equilibrium at the average gas temperature (1776°K). The symmetry of the discharge pattern in an asymmetric field indicates that the left and right boundaries of the mesh system are distant enough not to affect the current distribution. The electron density distributions show that inhomogeneities caused by the finite electrode segmentation diminish rapidly as one moves away from the walls.

A representative current distribution corresponding to $n_{e0} = 10^{13}$ cm^{-3} and $v_0 = 100$ m/sec ($\langle v \rangle = 88$ m/sec) is shown in Fig. 2. The three electron density distributions shown in the same figure for $y/H = \frac{1}{6}$ correspond to the same gas velocity but to three different n_{e0} values. The curve at the top corresponds to Saha density at the average gas temperature. As can be seen, the current streamline distribution is no longer symmetric, the current streamlines—particularly from the last electrode pair—are swept in the downstream direction. The dotted lines on the electon density plots correspond to Saha values defined by the local electron temperature. The electron density fluctuation lags behind the electron tempera-

Table 1 Reduced effective internal resistance $\langle E_y \rangle / E_{yid}$ ($\langle J_y \rangle$ = const) of the individual electrode pairs as a function of the gas velocity and inlet electron density

Gas velocity, m/sec	Electrode pair number	Inlet electron density, cm^{-3}		
		10^{12}	10^{13}	10^{14}
$v_0 \approx 0$	1	1.19	...	...
$\langle v \rangle \approx 0$	2	1.18	...	...
	3	1.18	...	...
	4	1.19	...	...
$v_0 = 100$	1	1.60	1.53	1.52
$\langle v \rangle = 88$	2	1.11	1.11	1.11
	3	1.11	1.11	1.10
	4	1.02	1.00	0.99
$v_0 = 250$	1	2.02	1.78	1.31
$\langle v \rangle = 220$	2	1.28	1.18	1.17
	3	1.15	1.13	1.10
	4	1.02	1.00	1.00
$v_0 = 500$	1	2.56	2.11	1.18
$\langle v \rangle = 440$	2	1.42	1.23	1.18
	3	1.18	1.15	1.14
	4	1.05	1.05	1.00

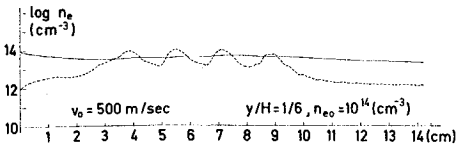

Fig. 3 Electron density distribution at $v_0 = 500$ m/sec and $n_{e0} = 10^{14}$ cm^{-3}.

ture fluctuations, particularly at lower electron densities. The typical relaxation length at this velocity is about 2 cm. The results of computations show that the locus of maximum current density roughly coincides with that of maximum electron density, but is shifted slightly (1–2 mm at the gas velocities considered here) to the side of the maximum electron temperature. Hence, higher electron density on the upstream side of a discharge tends to "pull" the current streamlines forward, thus partially compensating the velocity-sweep. At 100 m/sec gas velocity, the current density distribution remains nearly the same for all three inlet electron density values (the electron densities are approximately the same for $x \gtrsim 3$ cm). The sharp increase of the electron temperature observed in front of the first electrode pair at low inlet electron densities gradually reduces as the inlet electron density increases. This phenomenon, i.e., the necessity for higher electron temperatures at lower electron densities to carry the same current, has been observed experimentally.[6]

The effect of preionization and gas velocity on the performance characteristics of MHD devices can be seen from the data in Table 1. Here the ratio of average to ideal Faraday field strength is given for each electrode pair as function of the preionization level (inlet electron density) and gas velocity. Since the current flow through each electrode pair is kept constant, the ratio $\langle E_y \rangle / E_{y\mathrm{id}}$ is a measure of the "local" (per electrode pair) effective internal resistance of the generator. The quantities appearing in this table arre defined as follows: $\langle E_y \rangle = (1/H)_H \int E_y dy$, $E_{y\mathrm{id}} = \langle v \rangle B + \langle J_y \rangle / \sigma_{\mathrm{id}}$ and σ_{id} is the nonequilibrium conductivity value defined by the average current density under ideal conditions (zero losses, Saha equilibrium, etc.).

As can be seen, at low inlet electron densities the internal resistance increases monotonically with increasing velocity, but only the first few electrode pairs are affected appreciably by the velocity changes. Comparing the cases $v \approx 0$ and $\langle v \rangle = 440$ m/sec ($n_e = 10^{12}$ cm^{-3}), the effective internal resistances differ by a factor of 2.5 at the first electrode pair. At low gas velocities an increase of the inlet electron density has no pronounced effect on the generator performance because the electrons recombine before they reach the first electrode pair. Only when the plasma velocity is high enough and the typical relaxation length exceeds the distance between the preionizer and the first electrode pair does the effect of a high inlet electron density become highly pronounced (compare the case $v_0 = 500$ m/sec, $n_e = 10^{14}$ cm^{-3} with the others in Table 1). This can also be seen by comparing the last electron density distribution of Fig. 2 with Fig. 3: although at $v_0 = 100$ m/sec the electron density first decreases (recombination effect) and then, due to ohmic heat input, increases again in the region of the first electrode pair, at $v_0 = 500$ m/sec it does not succeed in recombining nor in following the electron temperature fluctuations and remains practically constant in the entire active zone of the duct. The corresponding reduction of the effective internal resistance is apparent.

References

[1] Lengyel, L. L., "Computation of Current Distributions in MHD Generators with Allowance for Recombination Effects," *Proceedings of the Eighth Symposium on Engineering Aspects of Magnetohydrodynamics*, Stanford Univ., March 1967, pp. 105–106; also *Energy Conversion*, Vol. 9, 1969, pp. 13–23.

[2] Oliver, D. A. and Mitchner, M., "Nonuniform Electrical Conduction in MHD Channels," *AIAA Journal*, Vol. 5, No. 8, Aug. 1967, pp. 1424–1432.

[3] Lengyel, L. L., "Numerical Simulation of Ionization Instability with Allowance for Dissipative Processes," *Proceedings of the Eleventh Symposium on Engineering Aspects of Magnetohydrodynamics*, California Institute of Technology, March 1970, pp. 193–198.

[4] Cool, A. T. and Zukoski, A. E., "Recombination; Ionization and Nonequilibrium Electrical Conductivity in Seeded Plasmas," *The Physics of Fluids*, Vol. 9, No. 4, April 1966, pp. 780–796.

[5] Kerrebrock, J. L. and Hoffman, M. A., "Nonequilibrium Ionization due to Electron Heating, Pt. II: Experiments," *AIAA Journal*, Vol. 2, No. 6, June 1964, pp. 1080–1087.

[6] Dodel, G., "Experimental Investigaion of Current Density Distributions in an Argon-Potassium Plasma Streaming through a Channel with Segmented Electrodes," *Plasma Physics*, Vol. 12, 1970, pp. 273–292.

Suboptimal Linear Filtering with a Limited State

JOHN R. HATFIELD*
Massachusetts Institute of Technology, Cambridge, Mass.
AND
DONALD ROCKWELL†
Boston University, Boston, Mass.
AND
PAUL ABRAMSON‡
Transportation Systems Center, Cambridge, Mass.

I. Introduction

IN applying Kalman filtering theory to real time filtering problems, it is often found impractical to estimate the complete state every time a measurement is made. In this case, one is forced to settle for some form of suboptimal filtering in which the dimension of the filter state is limited. If the filtering gains are being computed in real time, this problem can sometimes be solved by simplifying the model and perhaps modifying the driving noise and/or the measurement noise to try to compensate in some way for this simplification. The case considered here is the one in which the filtering gains are to be precomputed and stored in the computer. No restriction is placed on the method used to perform these computations, but there is a restriction on the number of gains that can be stored.

If the complete state is not being estimated, and one attempts to find a "best" set of gains to estimate the partial state recursively, the performance of the resulting filter can be very surprising. The purpose of this note is to illustrate some of these difficulties in the context of a simple example problem.

II. Statement of the Problem

Consider an aircraft flying towards a landing site at a known constant velocity. It is desired to estimate the range to go with radar range measurements that contain errors due to an unknown scale factor as well as wideband (white) measurement noise. Although the actual measurements, which can be written as the product of the range and scale factor plus the

Received October 13, 1970; revision received December 28, 1970. The authors wish to acknowledge the many stimulating discussions of this work that they enjoyed with their colleagues at the NASA Electronics Research Center. Particular credit is due to J. Canniff for programing the necessary computations.

* Staff Member, Man-Vehicle Laboratory. Member AIAA.
† Assistant Professor, College of Engineering. Member AIAA.
‡ Chief, Navigation and Guidance Branch.